Available online at www.sciencedirect.com
ScienceDirect
Journal of Sound and Vibration 318 (2008) 74–92
JOURNAL OF SOUND AND VIBRATION
www.elsevier.com/locate/jsvi

Active aeroelastic control of aircraft composite wings impacted by explosive blasts

Liviu Librescu[a], Sungsoo Na[b,*], Zhanming Qin[c], Bokhee Lee[b]

[a]*Department of Engineering Science and Mechanics, Virginia Polytechnic Institute and State University, Blacksburg, VA 24061, USA*
[b]*Department of Mechanical Engineering, Korea University, 1,5-ga, Anam-dong, Seongbuk-gu, Seoul 136-713, South Korea*
[c]*School of Aerospace, Xi'an, Jiaotong University, Xi'an, Shaanxi Province, 710049, China*

Received 19 June 2007; received in revised form 5 April 2008; accepted 7 April 2008
Handling Editor: J. Lam
Available online 27 May 2008

Abstract

In this paper, the dynamic aeroelastic response and the related robust control of aircraft swept wings exposed to gust and explosive type loads are examined. The structural model of the wing is in the form of a thin/thick-walled beam and incorporates a number of non-standard effects, such as transverse shear, material anisotropy, warping inhibition, the spanwise non-uniformity of the cross-section, and the rotatory inertias. The circumferentially asymmetric stiffness lay-up configuration is implemented to generate preferred elastic couplings, and in this context, the implications of the plunging–twist elastic coupling and of warping inhibition on the aeroelastic response are investigated. The unsteady incompressible aerodynamic theory adopted in this study is that by von-Kármán and Sears, applicable to arbitrary small motion in the time domain. The considered control methodology enabling one to enhance the aeroelastic response in the subcritical flight speed range and to suppress the occurrence of the flutter instability is based on a novel control approach that is aimed to improve the robustness to modeling uncertainties and external disturbances. To this end, a combined control based on Linear Quadratic Gaussian (LQG) controller coupled with the Sliding Mode Observer (SMO) is designed and its high efficiency is put into evidence.

1. Introduction

The next generation of advanced flight vehicles, and especially the military ones, are likely to operate in more severe environmental conditions than in the past. In this connection, the study of dynamic aeroelastic response and robust control of their aircraft wings to time-dependent external loadings, such as gust, sonic-boom and explosive induced blast is highly demanded. The significance of present research is closely related not only to the goal of improving the operational qualities of these flight vehicles, but also with that of the avoidance of structural failure by fatigue, and even of their catastrophic failure, when, in special instances, such as escape maneuvers, the combat aircraft is crossing the flutter boundary. In spite of the

*Corresponding author. Tel.: +82 2 3290 3370; fax: +82 2 926 9290.
E-mail addresses: librescu@vt.edu (L. Librescu), nass@korea.ac.kr (S. Na), zhanming.qin@gmail.com (Z. Qin), greensmile@korea.ac.kr (B. Lee).

0022-460X/$ - see front matter © 2008 Elsevier Ltd. All rights reserved.
doi:10.1016/j.jsv.2008.04.007

Nomenclature

AR	wing aspect ratio, L/b
a_{ij}	one-dimensional stiffness coefficient
b	semiwidth of the beam cross-section
$C_{L\phi}$	local life curve slope
F_ω , $r_t(s)$	primary and secondary warping functions, respectively
G_{sy}	effective membrane shear stiffness
$h_{(k)}$, h	thickness of the kth layer and thickness of the wall, respectively
L_{ae}	unsteady aerodynamic loads
L_g, L_b	aerodynamic loads due to gust and blast, respectively
M_x, M_y	one-dimensional stress couples
m	number of truncated modes used for the calculation
N	number of polynomials used in the shape function
n	number of aerodynamic lag terms used in the approximation of Wagner's function
P_0	peak reflected overpressure
Q_z	transverse shear force in the z direction
r	pulse length factor
U_n	chordwise freestream speed, defined as $U_\infty \cos \Lambda$
U_∞	streamwise freestream speed
V_G	peak gust velocity
w_0, ϕ	deflection, rotation about the reference axis
$\hat{w}_0, \hat{\phi}, \hat{\theta}_x$	non-dimensionalized counterparts of w_0, ϕ, θ_x
θ_x	rotation of the cross-section about x-axis
$[\theta_n]$	lay-up scheme
Λ	sweep angle
ρ_∞	mass density of the freestream
τ	non-dimensional time variables, defined as $U_n\, t/b$
τ_p	positive phase duration of the pulse
ϕ_∞	Wagner's function
$\hat{\Psi}_\omega, \hat{\Psi}_\phi, \hat{\Psi}_x$	admissible shape functions vectors with dimension $N \times 1$
ψ_k	Küssner's function
$\oint_c, \int_0^L$	integral along the cross-section and the span, respectively
$\int_{-b}^{b}, \int_{-1}^{1}$	airfoil integrals
$[\dot{(\,)}(\ddot{\,})]$	$[\partial(\,)/\partial t, \partial^2(\,)/\partial^2 t]$
$[(\,)', (\,)'']$	$[\partial(\,)/\partial y, \partial^2(\,)/\partial y^2]$

evident practical importance of the problems of the aeroelastic response and control of flight vehicle structures subjected to blast-type pressure pulses, the specialized literature is very scanty. In this sense, the reader is referred to the most authoritative survey papers, Refs. [1,2] and also Ref. [3], where the status of these problems has been presented. It should be mentioned that, in the context of aeroelastic response to blast loads, the main available results have concerned the aeroelastic response of 2-D airfoils without incorporation of any control capability (see e.g. Refs. [4–8] while for 3-D wings, the problem considered in the same spirit was addressed in Ref. [9]. In this paper, the approach of the problem is carried out in a broader context, in the sense that the aircraft wing is modeled as an anisotropic composite thin/thick-walled beam that encompasses a number of non-classical features. Moreover, a novel robust control approach intended to improve robustness to modeling uncertainties and external disturbances, to alleviate the aeroelastic response in the subcritical flight speed regime and expand the flight envelope by postponing the occurrence of the flutter instability is presented. The results show that the proposed performances are superior to those based on classical robust methodologies based solely on Kalman filter observer.

2. The structural model and the governing system

2.1. Kinematic equations

Toward the study of the aeroelastic response and feedback control of advanced aircraft wings, the concept of single-cell, closed cross-section composite anisotropic thin/thick-walled beam is used. The considered beam model incorporates a number of non-classical effects, such as anisotropy of constituent materials, transverse shear, warping inhibition, plunging–twist elastic coupling, contourwise shear stiffness variation, and spanwise non-uniformity of the wing cross-section. In various contexts, these effects have been accounted for in

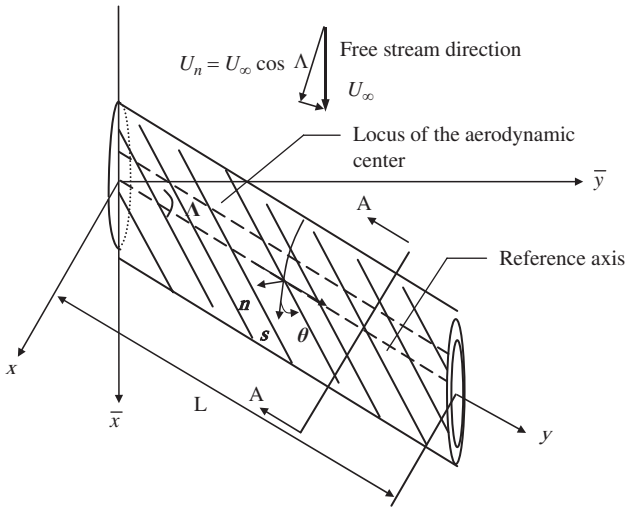

Fig. 1. Geometry of the aircraft wing modeled as a thin/thick-walled beam.

Ref. [10] through [11], and especially in monograph [12], where their implications have been assessed and validated. It should also be mentioned that in the context of an advanced composite *solid beam* model, problems of aircraft wing aeroelastic instability have been considered in Refs. [13–15]. The wing structure, modeled as a single-cell of a symmetric bi-convex cross-section is represented in Fig. 1. Its points are referred to the global coordinate system (x, y, z) with its origin at the wing root. Coordinates x and y constitute the chordwise (positive rearward) and the spanwise one, respectively, while z is the coordinate normal to plane (x, y), positive upward. In addition, a local coordinate system (s, y, n) is adopted, where s and n are the circumferential and the transversal ones, respectively. Based on the assumptions stipulated in Ref. [12], the following representation for the 3-D displacement quantities is considered:

$$\begin{aligned} u(x,y,z,t) &= u_0(y,t) + \underline{z\phi(y,t)}\,, \\ v(x,y,z,t) &= v_0(y,t) + \left[x(s) - n\frac{\mathrm{d}z}{\mathrm{d}n}\right]\theta_z(y,t) \\ &\quad + \left[z(s) + n\frac{\mathrm{d}x}{\mathrm{d}z}\right]\theta_x(y,t) - \underline{[F(s) - nr_t(s)]\phi'(y,t)}\,, \\ w(x,y,z,t) &= \underline{w_0(y,t)} - \underline{x\phi(y,t)}, \end{aligned} \qquad (1a - c)$$

where

$$\underline{\theta_x(y,t)} = \underline{\gamma_{yz}(y,t)} - \underline{w_0'(y,t)} \quad \text{and} \quad \theta_z(y,t) = \underline{\gamma_{xy}(y,t)} - \underline{u_0'(y,t)}\,. \qquad (2)$$

In the above expressions, $\underline{\theta_x(y,t)}$, $\underline{\theta_z(y,t)}$ and $\underline{\phi(y,t)}$ denote the rotations of the cross-section about the axes x, z, and the twist about the y-axis, respectively; $\underline{\gamma_{yz}(y,t)}$ and $\underline{\gamma_{xy}(y,t)}$ denote the transverse shear strain measures, while $\underline{v_0(y,t)}, \underline{u_0(y,t)}$ and $\underline{w_0(y,t)}$ denote the spanwise, lateral and transversal displacements of the wing reference line, respectively.

The primary and secondary warping functions in Eq. (1b) are expressed as (see Refs. [11,12])

$$\begin{aligned} F_w(s) &= \int_0^s [r_n(s) - \psi(s)]\mathrm{d}s, \\ r_t(s) &= -\left(z\frac{\mathrm{d}z}{\mathrm{d}s} + x\frac{\mathrm{d}x}{\mathrm{d}s}\right) \end{aligned} \qquad (3)$$

in which the torsional function $\psi(s)$ and the geometrical quantity r_n(s) are as follows:

$$\psi(s)=\frac{\oint_C r_n(\bar{s})\mathrm{d}\bar{s}}{h(s)G_{sy}(s)\oint_C \dfrac{\mathrm{d}\bar{s}}{h(\bar{s})G_{sy}(\bar{s})}},\quad r_n(s)=z\frac{\mathrm{d}x}{\mathrm{d}s}-x\frac{\mathrm{d}z}{\mathrm{d}s}, \tag{4a,b}$$

where G_{sy}(s) is the effective contourwise membrane shear stiffness defined as

$$G_{sy}(s)=\frac{N_{sy}}{h(s)\gamma^0_{sy}(s)}. \tag{5}$$

It is noted that for the general thin/thick-walled beam theory, the six kinematic variables, $u_0(y,t)$, $v_0(y,t)$, $w_0(y,t)$, $\theta_x(y,t)$, $\theta_z(y,t)$, $\phi(y,t)$ that represent 1-D displacement measures, constitute the basic unknowns of the problem. When transverse shear effect is discarded, Eqs. (2) reduce to $\theta_x=-w_0'$, $\theta_z=-u_0'$, and as a result, the number of basic unknown quantities reduces to four. Such a case leads to the classical, unshearable beam model.

In the case of the aeroelasticity of aircraft wings featuring a symmetric bi-convex cross-section and experiencing bending–twist elastic coupling, a specific lay-up architecture, referred to as the *circumferentially asymmetric stiffness* (CAS) configuration will be adopted [10,12,16]. In its context, the aeroelastic governing equations are exactly and entirely decoupled into two groups: (i) vertical bending (plunging)/twist (pitch)/vertical transverse shear expressed in terms of 2-D displacement measures, $w_0(y,t)$, $\phi(y,t)$ and $\theta_x(y,t)$, and (ii) extension/lateral bending/lateral transverse shear, expressed in terms of displacement quantities $u_0(y,t)$, $v_0(y,t)$ and $\theta_y(y,t)$. As is evident, only the former set of elastic couplings is relevant for the present problem, and, as a result, the problem involving the latter ones will not be considered. In order to better distinguish the terms that are proper to the problem at hand, in Eqs. (1) these were underscored by a solid line.

In order to be reasonably self-contained, the basic equations that yield the pertinent governing equations will be summarized.

The strain quantities, restricted to those that are relevant to the present problem are:

Spanwise strain component:

$$\varepsilon_{yy}(n,s,y,t)=\varepsilon^{(0)}_{yy}(s,y,t)+n\varepsilon^{(1)}_{yy}(s,y,t), \tag{6a}$$

where

$$\varepsilon^{(0)}_{yy}(s,y,t)=v_0'(y,t)+\theta_z'(y,t)x(s)-\underline{\phi''(y,t)F_w(s)}, \tag{6b}$$

$$\varepsilon^{(0)}_{yy}(s,y,t)=v_0'(y,t)+\theta_z'(y,t)x(s)+\theta_x'(y,t)z(s)-\phi''(y,t)F_w(s),$$

$$\varepsilon^{(1)}_{yy}(s,y,t)=-\theta_z'(y,t)\frac{\mathrm{d}z}{\mathrm{d}s}+\underline{\theta_x'(y,t)\frac{\mathrm{d}x}{\mathrm{d}s}}-\underline{r_t(s)\phi''(y,t)} \tag{6c}$$

are the axial strain components associated with the primary and secondary warping, respectively.

The tangential shear strain:

$$\gamma_{sy}(s,y,t)=\underline{\gamma^0_{sy}(s,y,t)}+\underline{\psi(s)\phi'(y,t)}, \tag{7a}$$

where

$$\gamma^0_{sy}(s,y,t)=\gamma_{xy}\frac{\mathrm{d}x}{\mathrm{d}s}+\underline{\gamma_{yz}\frac{\mathrm{d}z}{\mathrm{d}s}}=\left[u_0'+\theta_z\right]\frac{\mathrm{d}x}{\mathrm{d}s}+\underline{\left[w_0'+\theta_x\right]\frac{\mathrm{d}z}{\mathrm{d}s}}. \tag{7b}$$

The transverse shear strain:

$$\gamma_{ny}(s,y,t)=-\gamma_{xy}\frac{\mathrm{d}z}{\mathrm{d}s}+\underline{\gamma_{yz}\frac{\mathrm{d}x}{\mathrm{d}s}}=-\left[u_0'+\theta_z\right]\frac{\mathrm{d}z}{\mathrm{d}s}+\underline{\left[w_0'+\theta_x\right]\frac{\mathrm{d}x}{\mathrm{d}s}}. \tag{8}$$

In their expressions, the same convention of underscoring the terms pertinent to bending–twist coupling was adopted.

2.2. The governing system

The governing equations and boundary conditions that should be consistent with the previously displayed kinematical equations are derived via the Extended Hamilton's Principle. It states that the true path of motion renders the following variational form stationary:

$$\int_{t_1}^{t_2}(\delta T-\delta V+\overline{\delta W_e})\mathrm{d}t=0, \tag{9a}$$

with

$$\delta w_0=\delta\theta_x=\delta\phi=0 \quad \text{at } t=t_1,t_2, \tag{9b}$$

where T and V denote the kinetic energy and strain energy, respectively, $\overline{\delta W_e}$ denotes the virtual work due to external forces, while t_1 and t_2 are two arbitrary instants of time. The energy quantities intervening in Eq. (9a) are as follows:

Kinetic energy:

$$T=\frac{1}{2}\int_0^L\oint_C\sum_{k=1}^{m_1}\int_{h_{(k)}}\rho_{(k)}\left[\left(\frac{\partial u}{\partial t}\right)^2+\left(\frac{\partial w}{\partial t}\right)^2+\left(\frac{\partial v}{\partial t}\right)^2\right]\mathrm{d}n\,\mathrm{d}s\,\mathrm{d}y, \tag{10}$$

Strain energy:

$$\begin{aligned}V&=\frac{1}{2}\int_\tau\sigma_{ij}\varepsilon_{ij}\mathrm{d}\tau\\&=\frac{1}{2}\int_0^L\oint_C\sum_{k=1}^{m_1}\left[\sigma_{yy}\varepsilon_{yy}+\sigma_{sy}\gamma_{sy}+\sigma_{ny}\gamma_{ny}\right]_{h_{(k)}}\mathrm{d}n\mathrm{d}s\mathrm{d}y,\end{aligned} \tag{11}$$

Virtual work due to unsteady aerodynamic, gust, blast and control loads:

$$\overline{\delta W_e}=\int_0^L(p_z(y,t)\delta w_0(y,t)+m_y(y,t)\delta\phi(y,t))\mathrm{d}y, \tag{12}$$

where $p_z=L_{ae}+\delta_g L_g+\delta_b L_b+L_c$ (positive upwards) stands for the combined aerodynamic, blast/gust and control lift per unit span length, while $m_y=T_{ae}+T_g+T_c$ (positive nose-up) denote the combined aerodynamic and related induced twist moments about the reference axis. The two tracers δ_g and δ_b take the values 1 or 0, when the gust or blast effects are included or discarded respectively. In the present numerical simulations, when $\delta_g=1$, $\delta_b=0$, and vice-versa.

As it was already stated, we consider that the aircraft wing features a bi-convex cross-section experiencing the bending–twist coupling. The equations of motion pertinent to this case are as follows:

$$\begin{aligned}&\delta w_0: Q_z'+L_{\mathrm{ae}}+L_g+L_c-b_1\ddot{w}_0=0,\\&\delta\phi: M_y'-B_w''+T_{\mathrm{ae}}+T_g+T_c-(b_4+b_5)\phi''+(b_{10}+b_{18})\ddot{\phi}''=0,\\&\delta\theta_x: M_x'-Q_z-(b_4+b_{14})\ddot{\theta}_x=0,\end{aligned} \tag{13a - c}$$

with the boundary conditions for the case of the wing clamped at $y=0$

$$w_0=0,\quad \phi=0,\quad \phi'=0,\quad \theta_x=0$$

and free at $y=L$

$$Q_z=0,\quad -B_w'+M_y+(b_{10}+b_{18})\ddot{\phi}'=0,\quad B_w=0,\quad M_x=0. \tag{14}$$

In the above equations, M_x, Q_z, B_w, M_y are the 1-D stress resultant and stress couple measures that are defined as

$$M_x(y,t)=\oint_C\left(zN_{yy}+L_{yy}\frac{\mathrm{d}x}{\mathrm{d}s}\right)\mathrm{d}s$$

$$Q_z(y,t) = \oint_C \left(N_{sy}\frac{\mathrm{d}z}{\mathrm{d}s} + N_{ny}\frac{\mathrm{d}x}{\mathrm{d}s}\right)\mathrm{d}s$$

$$B_w(y,t) = -\oint_C \left[F_w(s)N_{yy} + r_t(s)L_{yy}\right]\mathrm{d}s$$

$$M_y(y,t) = \oint_C N_{sy}\psi(s)\mathrm{d}s. \tag{15}$$

In addition, b_1, b_4, b_5, b_{10}, b_{14}, b_{15}, b_{18} are the inertia coefficients, while N_{yy}, N_{sy}, N_{ny}, L_{yy} are the 2-D stress resultant/couple measures.

In the previous equations, for the CAS lay-up configuration, the 1-D force–displacement relations are:

$$\begin{Bmatrix} M_x \\ Q_z \\ B_w \\ M_y \end{Bmatrix} = \begin{bmatrix} a_{33} & 0 & 0 & a_{37} \\ 0 & a_{55} & a_{56} & 0 \\ 0 & a_{56} & a_{66} & 0 \\ a_{37} & 0 & 0 & a_{77} \end{bmatrix} \begin{Bmatrix} \theta_x' \\ (w_0' + \theta_x) \\ \phi'' \\ \phi' \end{Bmatrix}. \tag{16}$$

While for the free warping wing model (see Refs. [9,12]), the force–displacement relations are:

$$\begin{Bmatrix} M_x \\ Q_x \\ B_w \\ M_y \end{Bmatrix} = \begin{bmatrix} a_{33} & 0 & a_{37} \\ 0 & a_{55} & 0 \\ 0 & a_{56} & 0 \\ a_{37} & 0 & a_{77} \end{bmatrix} \begin{Bmatrix} \theta_x' \\ (w_0' + \theta_x) \\ \phi' \end{Bmatrix}, \tag{17}$$

for the unshearable structural model, the counterpart of Eq. (16) is

$$\begin{Bmatrix} M_x \\ Q_z \\ B_w \\ M_y \end{Bmatrix} = \begin{bmatrix} a_{33} & 0 & a_{37} \\ 0 & a_{56} & 0 \\ 0 & a_{66} & 0 \\ a_{37} & 0 & a_{77} \end{bmatrix} \begin{Bmatrix} -w_0'' \\ \phi'' \\ \phi' \end{Bmatrix}. \tag{18}$$

Having in view that the assumption of the spanwise cross-section non-uniformity was adopted, the stiffness and inertia quantities, a_{ij} and b_{ij} are functions of spanwise coordinate. Their expression can be found in Refs. [9,12,17].

In terms of the basic unknowns, the governing equations that include spanwise non-uniformity, transverse shear, warping inhibition and rotatory inertias are:

$$\begin{aligned}
\delta w_0 &: \left[a_{55}(w_0' + \theta_x)\right]' + \underline{\underline{\left[a_{56}\phi''\right]'}} \\
&\quad + L_{\mathrm{ae}} + L_g + L_b + L_c - b_1\ddot{w}_0 = 0, \\
\delta\phi &: \left[a_{37}\theta_x'\right]' + \left[a_{77}\phi'\right]' - \left[a_{56}(w_0' + \theta_x)\right]'' - \underline{\underline{\left[a_{66}\phi''\right]''}} \\
&\quad + T_{\mathrm{ae}} + T_g + T_c - (b_4 + b_5)\ddot{\phi} + \underline{\underline{\left[(b_{10} + b_{18})\ddot{\phi}'\right]'}} = 0, \\
\delta\theta_x &: \left[a_{33}\theta_x'\right]' + \left[a_{37}\phi'\right]' - a_{55}(w_0' + \theta_x) \\
&\quad - \underline{\underline{a_{56}\phi''}} - \underline{\qquad (b_4 + b_{14})\ddot{\theta}_x \qquad} = 0,
\end{aligned} \tag{19a - c}$$

to which we associate the boundary conditions:

At $y = 0$

$$w_0 = 0, \quad \phi = 0, \quad \underline{\underline{\phi' = 0}}, \quad \theta_x = 0. \tag{20a}$$

At $y = L$,

$$\begin{aligned}
&\delta w_0 : a_{55}(w_0' + \theta_x) + \underline{\underline{a_{56}\phi''}} = 0,\\
&\delta\phi : -[a_{56}(w_0' + \theta_x)]' - [\underline{\underline{a_{66}\phi''}}]' + a_{37}\theta_x' + a_{77}\phi'\\
&\qquad = -(b_{10} + b_{18})\ddot{\phi}',\\
&\delta\phi' : -a_{56}(w_0' + \theta_x) - \underline{\underline{a_{66}\phi''}} = 0,\\
&\delta\theta_x : a_{33}\theta_x' + a_{37}\phi' = 0,
\end{aligned} \tag{20b}$$

where L denotes the semi-wing span.

In the above equations, the term underscored by a dashed and double underscored solid lines identify those related to the rotatory inertia and with the warping inhibition effect.

3. Unsteady aerodynamic loads for arbitrary small motion in incompressible flow

Based on the 2-D incompressible unsteady strip theory aerodynamics, the aerodynamic lift and twist moment about the reference axis (selected to coincide with the mid-chord line), can be expressed in the time domain as the superposition of three parts (see Ref. [18]):

$$\begin{aligned}
L_{ae}(y,t) = &-\rho_\infty \frac{d}{dt}\int_{-b}^{b}\gamma_0(x,y,t)x\,dx + \rho_\infty U_n \Gamma_0(y,t)\\
&+\rho_\infty U_n \int_{-b}^{\infty}\frac{\gamma_w(x,y,t)}{\sqrt{x^2-b^2}}\,dx,\\
T_{ae}(y,t) = &+\frac{1}{2}\rho_\infty \frac{d}{dt}\int_{-b}^{b}\gamma_0(x,y,t)(x^2-\frac{1}{2}b^2)dx\\
&-\rho_\infty U_n \int_{-b}^{b}\gamma_0(x,y,t)x\,dx + \frac{1}{2}\rho_\infty U_n b^2 \int_{-b}^{\infty}\frac{\gamma_w(x,y,t)}{\sqrt{x^2-b^2}}dx,
\end{aligned} \tag{21a,b}$$

where U_n is the free stream speed normal to the leading edge, $\gamma_0(x,y,t)$ is the quasi-steady distributed bound vortex intensity (on the wing), $\gamma_w(x,y,t)$ is the vortex intensity in the wake, and $\Gamma_0(y,t)$ is the quasi-steady circulation. From the aerodynamic potential theory, $\gamma_0(x,y,t)$, $\gamma_w(x,y,t)$ can be uniquely determined by the boundary (no-penetration) condition and the Kutta condition, as illustrated in the following.

Expressed in the body-fixed frame as represented in Fig. 1, (see Refs. [19,20] and also Refs. [9,17]) the vertical position of the wing cross-section can be expressed as

$$z_a(x,y,t) = w_0(y,t) - \phi(y,t)x, \tag{22}$$

where $w_0(y,t)$ and $\phi(y,t)$ denote the plunging displacement of the points associated with the reference axis, and the twist about this axis, respectively.

Following the developments in Ref. [18] considered in conjunction with those in Ref. [19], the aerodynamic loads can be separated into two parts: the quasi-steady part and the part taking into account the influence of the wake. As a result, we get

$$\begin{aligned}
\Gamma_0(y,t) &= -2b\int_{-1}^{1}\sqrt{\frac{1+\hat{\xi}}{1-\hat{\xi}}}\left[\dot{w}_0 - U_n\phi - b\hat{\xi}\dot{\phi}\right]d\hat{\xi}\\
&= -2\pi\left[\dot{w}_0 - U_n\phi - \frac{1}{2}b\dot{\phi}\right] \underline{\Delta} -2\pi b w_{0.75c}(y,t),
\end{aligned}$$

$$
\begin{aligned}
L_{\mathrm{ae}}(y,t) = & -\pi\rho_\infty b^2[\dot{w}_{0.5c}(y,t)] \\
& -\underline{2\pi\rho_\infty U_n b\left\{w_{0.75c}(y,0)\phi_w\left(\frac{U_n t}{b}\right)+\int_0^t \frac{\mathrm{d}w_{0.75c}(t_0)}{\mathrm{d}t_0}\phi_w\left(\frac{U_n}{b}(t-t_0)\right)\mathrm{d}t_0\right\}}, \\
T_{\mathrm{ae}}(y,t) = & -\pi\rho_\infty b^3\left[\frac{1}{2}U_n\dot{\phi}+\frac{1}{8}b\ddot{\phi}\right] \\
& -\underline{\pi\rho_\infty U_n b^2\left\{w_{0.75c}(y,0)\phi_w\left(\frac{U_n t}{b}\right)+\int_0^t \frac{\mathrm{d}w_{0.75c}(t_0)}{\mathrm{d}t_0}\phi_w\left(\frac{U_n}{b}(t-t_0)\right)\mathrm{d}t_0\right\}}, \qquad (23\mathrm{a}-\mathrm{c})
\end{aligned}
$$

where the underscored terms are associated with the circulatory part of aerodynamic loads; ϕ_w is Wagner's function in the time domain that is the counterpart of Theodorsen's function in the frequency domain, (related to the latter one through an inverse Laplace transform), while $w_{0.75}$ and $w_{0.5}$ denote the downwash at the $\frac{3}{4}$ and $\frac{1}{2}$ chord points measured from the leading edge of the airfoil.

The above results are for 2-D cross-section wings. For a finite-span wing, the modified strip theory is used to extend the 2-D aerodynamics to the 3-D one [21,22]. To this end, in order to be able to capture also the case of swept aircraft wings, the reference coordinate system is being rotated with the wing by the sweep angle Λ (see e.g. Ref. [23]). In addition, the lift curve slope 2π and the downwash boundary condition for the 2-D aerodynamics model are modified to account for the finite-span effects [19,21,22]:

$$
2\pi \to C_{L\phi} \equiv \frac{\mathrm{d}C_L}{\mathrm{d}\phi} = \frac{\mathrm{AR}}{\mathrm{AR}+2\cos\Lambda}2\pi, \quad \frac{1}{2}b \to b\left[\frac{C_{L\phi}}{2\pi}-\frac{1}{2}\right]. \qquad (24)
$$

Related to Eqs. (23b,c), only the *circulatory* terms should be modified, and in connection with the geometric transformations, these are carried out in the rotated chordwise coordinate system (see Fig. 1).

As to the frame transformation, the procedure in Refs. [19,23] is followed here. After collecting the coefficients related to the chordwise coordinate x, the downwash in the rotated coordinate system is expressed as

$$
\begin{aligned}
w_a(x,y,t) &\cong \frac{\partial z_a}{\partial t}+\frac{\partial z_a}{\partial \bar{x}} = \frac{\partial z_a}{\partial t}+U_\infty\left(\frac{\partial z_a}{\partial x}+\frac{\partial z_a}{\partial y}\sin\Lambda\right) \\
&= \left[\dot{w}_0 - U_\infty\phi\cos\Lambda + U_\infty\sin\Lambda\frac{\partial w_0}{\partial y}\right] - x\left[\dot{\phi}+U_\infty\frac{\partial\phi}{\partial y}\sin\Lambda\right]. \qquad (25)
\end{aligned}
$$

Replacing in the previous equation $\dot{w}_0 - U_n\phi$ by $\dot{w}_0 - U_\infty\phi\cos\Lambda + U_\infty\sin\Lambda(\partial w_0/\partial y)$; $\dot{\phi}+U_\infty(\partial\phi/\partial y)\sin\Lambda$, and denoting $U_n \equiv U_\infty\cos\Lambda$, we get the downwash velocities at $\frac{3}{4}$ and $\frac{1}{2}$ chord points of the profile as

$$
\begin{aligned}
w_{0.75c}(y,t) &= \dot{w}_0 - U_n\phi + U_n\tan\Lambda\frac{\partial w_0}{\partial y} \\
&\quad -\frac{b}{2}\left[\dot{\phi}+U_n\frac{\partial\phi}{\partial y}\tan\Lambda\right]\left[\frac{C_{L\phi}}{\pi}-1\right], \\
w_{0.5c}(y,t) &= \dot{w}_0 - U_n\phi + U_n\tan\Lambda\frac{\partial w_0}{\partial y}. \qquad (26)
\end{aligned}
$$

4. Blast loads

The structure of combat aircraft or of space vehicles can be exposed during their operational life to blast pulses generated by an explosion, or by shock-wave disturbances produced by an aircraft flying at supersonic speeds, or by any supersonic projectile, rocket or missile operating in its vicinity.

In the latter case, the blast pulse is referred to as sonic-boom. Its time-history is described as an N-shape pulse, featuring both a positive and a negative phase. Having in view the large blast front generated by the explosion as compared to the dimensions of the wing, one assumes with sufficient accuracy that the pressure is uniform over the entire wing span and chord, and the impact is at normal incidence.

The sonic-boom overpressure can be expressed as follows (see e.g. (28)):

$$L_b(t) = \begin{cases} P_0(1 - t/t_p) & \text{for} \quad 0 < t < rt_p \\ 0 & \text{for} \quad t < 0 \text{ and } t > rt_p \end{cases} \tag{27}$$

where P_0 denotes the peak reflected pressure in excess to the ambient one, t_p denotes the positive phase duration of the pulse measured from the time of impact of the structure, and r denotes the shock pulse length factor.

For $r = 1$, the sonic-boom degenerates into a triangular explosive pulse, for $r = 2$, a symmetric sonic-boom pulse is obtained, while $r \neq 2$ corresponds to a non-symmetric N-pulse. When $r = 1$ and $t_p \to \infty$, in Eq. (27) the N-pulse degenerates in a step pulse.

For the blast pulse generated in an explosion, the overpressure is expressed in terms of Friedländer's exponential decay equation as [24,25]

$$L_b(t) = P_0\left(1 - \frac{t}{t_p}\right) \exp(-a' t/t_p) \tag{28}$$

where the negative phase of the blast is included. In Eq. (28), a' denotes a decay parameter that has to be adjusted as to approximate the pressure curve from the blast test. As it could be inferred, the triangular explosive blast pulse may be viewed as a limiting case of Eq. (28), for $a'/t_p \to 0$. As it can be realized (see also Ref. [25]), the latter case provides the most severe explosive blast load scenario.

The aeroelastic response to gusts will be also addressed here, and related with it, the concept of Küssner's function associated wit the gust penetration effects will be used. Such effects are initiated by the changes in the effective angle-of-attack due to the change in the flow direction. If we consider $w_G(\tau)$ as a gust variable velocity, then, the lift due to the penetration into a gust is given by

$$L_g(\tau) = C_{L\phi} b \rho U_\infty \left\{ w_G(0)\psi(\tau) + \int_0^T \partial w_G(\tau_0)/\partial\tau_0 \psi(\tau - \tau_0) \mathrm{d}\tau_0 \right\}, \tag{29}$$

where $\psi(\tau)$ is Küssner's function. Its approximate expression, derived by von-Kármán and Sears and reported in Ref. [19] for elliptic wings in an incompressible flow is $\Psi(\tau) = 1 - 0.500^{-0130\tau} - 0.500^{-\tau}, \quad (\tau > 0)$.

In the following developments, Küssner's function derived for sharp-edge gusts will be used to determine the aeroelastic response to gusts of different shapes. This will be carried out via the use of Duhamel's integral concept. Herein, the gust velocity distribution corresponding to a sharp-edge gust will be used. In this case

$$w_G(\tau) = H(\tau) V_G, \tag{30}$$

where V_G is peak gust velocity, while $H(\,)$ is Heaviside's function. As concerns the twist moment about the reference axis induced by the gust, its expression is

$$T_g(\tau) = \frac{1}{2} b L_g(\tau) = \frac{1}{2} C_{L\phi} b^2 U_n \left[w_G(0)\psi_K(\tau) + \int_0^\tau \frac{\partial w_G(\tau_0)}{\partial \tau_0} \psi_K(\tau - \tau_0) \mathrm{d}\tau_0 \right]. \tag{31}$$

5. State-space representation of the governing system

Due to the non-conservative nature of the boundary value/eigenvalue problems and the high complexity arising from the structural model that incorporates non-classical features, it is appropriate to apply the spatial discretization and then cast the governing equations in state-space form. The spatial discretization is carried out via the use of the extended Galerkin's method (EGM) (see Refs. [12,26]). In addition, for the purpose of treating blast/gust type loads and control forces in a unified way, the temporal discretization is implemented. Details of this can be found in Refs. [9,17,27].

Next, we define the following basic dimensionless parameters:

$$\begin{gathered}\eta \equiv y/L, \quad \tau \equiv U_n t/b, \quad \mathrm{AR} \equiv L/b, \quad \hat{w}_0(\eta,\tau) \equiv w_0/2b, \\ \hat{\phi}(\eta,\tau) \equiv \phi(\eta,\tau), \quad \hat{\theta}_x(\eta,\tau) \equiv \theta_x(\eta,\tau), \quad \mathrm{d}(.)/\mathrm{d}\tau = (b/U_n)\mathrm{d}(.)/\mathrm{d}t\end{gathered} \tag{32}$$

while for the spatial discretization one uses the representation

$$\begin{aligned}\hat{w}_0(\eta,\tau) &= \hat{\mathbf{\Psi}}_w^{\mathrm{T}}(\eta)\hat{\mathbf{q}}_w(\tau) \;\; \hat{\phi}(\eta,\tau) = \hat{\mathbf{\Psi}}_\phi^{\mathrm{T}}(\eta)\hat{\mathbf{q}}_\phi(\tau), \\ \hat{\theta}_x(\eta,\tau) &= \hat{\mathbf{\Psi}}_x^{\mathrm{T}}(\eta)\hat{\mathbf{q}}_x(\tau),\end{aligned} \tag{33}$$

where the shape functions $\hat{\Psi}_w(\eta)$, $\hat{\Psi}_\phi(\eta)$, and $\hat{\Psi}_x(\eta)$ are only required to fulfill the geometric boundary conditions, while $\hat{q}_w(\eta)$, $\hat{q}_\phi(\eta)$, and $\hat{q}_x(\eta)$ are the $N \times 1$ generalized coordinates. Following the steps carried out in Refs. [9,17], the state-space form of the aeroelastic governing system results as

$$\begin{Bmatrix}\dot{\hat{\mathbf{x}}}_s \\ \dot{\hat{\mathbf{x}}}_a\end{Bmatrix} = \begin{bmatrix}\mathbf{A}_s & \mathbf{B}_s \\ \mathbf{B}_a\mathbf{A}_s & \mathbf{A}_a + \mathbf{B}_a\mathbf{B}_s\end{bmatrix}\begin{Bmatrix}\hat{\mathbf{x}}_s \\ \hat{\mathbf{x}}_a\end{Bmatrix} + \begin{bmatrix}\mathbf{0}_{m\times 1} \\ \overline{\mathbf{M}}_n^{-1} \\ \mathbf{D}_2\overline{\mathbf{M}}_n^{-1} \\ \vdots \\ \mathbf{D}_2\overline{\mathbf{M}}_n^{-1}\end{bmatrix}\{\mathbf{Q}_g + \mathbf{Q}_b\}, \tag{34}$$

or in a more compact form, see Refs. [9,17] as

$$\{\dot{\hat{\mathbf{X}}}\} = [\mathbf{A}]\{\hat{\mathbf{X}}\} + [\mathbf{B}_e]\{\mathbf{Q}_g + \mathbf{Q}_b\}. \tag{35}$$

In Eq. (34), m is the number of the structural mode actually used in the calculation, while n is the number of aerodynamic lag terms used in the approximation of Wagner function. In addition, $\mathbf{x}_s$ and $\mathbf{x}_a$ are $2m \times 1$, $nm \times 1$ vectors that describe the motion of the wing and unsteady aerodynamic loads on the wing, respectively, while $\mathbf{Q}_g$ and $\mathbf{Q}_b$ are the generalized gust and blast loads and the generalized control forces, respectively. The explicit expression of the involved matrices and vectors are supplied in the Appendix of Ref. [17].

6. Design of the LQG controller and sliding mode observer

Active vibration control of aircraft structures, in general, and that of aeroelastic phenomena featured by aeronautical flight vehicles, in particular, constitutes a topic playing an exceptional importance toward the avoidance of large oscillations in the subcritical flight speed range and the expansion of the flight envelope, achieved through the increase of the flutter speed.

Moreover, the advanced military aircraft is likely to operate in severe environmental conditions consisting of blast/explosive pressure pulses and shocks inducing large oscillations in the pre-flutter speed range that can jeopardize the precision of the aircraft mission and its life span. These facts fully underline the necessity of the implementation of an active control capability enabling one to suppress the oscillations in the shortest possible time and expand the flight envelope without weight penalties.

To control vibration of such structures, a controller with finite order was commonly used. A finite-dimensional control may be designed from a reduced-order model (ROM) of the continuous structure counterpart.

When a ROM based finite-dimensional controller is applied to a real structure, it stabilizes just a few modes among the infinite number of modes of the system. Stability of the residual modes is not guaranteed. The interaction between the residual modes and the controller may deteriorate the performance of the control system, and even cause instability. Due to its detrimental effects on performance of the closed-loop system, this phenomenon studied first by Balas [28] and known as spillover, was further investigated, and various approaches enabling one to suppress it have been proposed. In the context of the aeroelasticity of a supersonic airfoil, in Refs. [7,8] the feedback controls circumventing the problem of the spillover have been presented, while a number of comprehensive survey papers on this matter have been provided in Refs. [1,2].

Within this paper, an aeroelastic control approach of 3-D aircraft wings exposed to time-dependent external blasts and operating in an incompressible subcritical flow field will be investigated. Within this approach, the control is aimed at improving robustness to modeling uncertainties and external disturbances.

6.1. LQG controller

While the Linear Quadratic Regulator (LQR) design provides an optimal controller, this control methodology is not reliable because it uses the full state vector $\mathbf{X}$. Furthermore, due to the unavailable lag states or of unpredictable situations emerging, for example, as a result of the failure of sensors, an observer should be designed as to estimate the unavailable states. As a result, the feedback control scheme should be implemented via the estimated states.

In order to approach this problem, it is convenient to split the governing state-space system in controlled and uncontrolled parts as

$$\begin{aligned} \dot{\mathbf{X}}_C &= \mathbf{A}_C\mathbf{X}_C + \mathbf{B}_C\mathbf{u}, \\ \dot{\mathbf{X}}_R &= \mathbf{A}_R\mathbf{X}_R + \mathbf{B}_R\mathbf{u}, \\ \mathbf{y} &= \mathbf{C}_C\mathbf{X}_C + \mathbf{C}_R\mathbf{X}_R, \end{aligned} \tag{36a - c}$$

where $\mathbf{X}_C$ are the controlled mode states and $\mathbf{X}_R$ are the residual modes states, where the block matrices $\mathbf{A}_C$, $\mathbf{B}_C$. $\mathbf{C}_C$ and $\mathbf{C}_R$ are of appropriate dimensions to $\mathbf{X}_C$ and $\mathbf{X}_R$. Usually, a controller and an observer are designed based on the controlled mode system, Eq. (36a), ignoring the residual mode subsystem, Eq. (36b). In this sense, the LQG is designed as follows:

$$\begin{aligned} \dot{\tilde{\mathbf{X}}}_C(t) &= \mathbf{A}_C\tilde{\mathbf{X}}_C + \mathbf{B}_C\mathbf{u}(t) + \mathbf{L}\big[\mathbf{y}(t) - \mathbf{C}_C\tilde{\mathbf{X}}(t)\big], \\ \mathbf{u}(t) &= \mathbf{K}\tilde{\mathbf{X}}_C(t), \\ \tilde{\mathbf{y}}(t) &= \mathbf{C}_C\tilde{\mathbf{X}}_C, \end{aligned} \tag{37a - c}$$

where $\tilde{\mathbf{X}}_C$ denotes the estimated state based on input and output measurements, while $\mathbf{K}$ and $\mathbf{L}$ are the control gain matrix and the Kalman filter gain matrix, respectively. It clearly appears that the LQG method couples the Kalman filter with the LQR.

From Eqs. (36c) and (37c) it can be seen that the difference between the actual measurements $\mathbf{y}$ and the estimated ones $\tilde{y}$, referred to as the residual, is proportional to the error dynamics $\mathbf{e}(t) = \mathbf{X}(t) - \tilde{\mathbf{X}}(t)$. This implies that if the error would tend to zero, also the residuals will experience a similar trend.

Furthermore, one needs to consider the effects of process disturbances and of measurement noise. To address these issues, an LQG design, which uses noise-corrupted outputs for feedback is used as a controller. Using LQG method with plant disturbance and sensor noise, the associated equations representing the counterpart of Eqs. (36) are represented in state-space form as

$$\begin{aligned} \dot{\mathbf{X}}(t) &= \mathbf{A}\mathbf{X}(t) + \mathbf{B}\mathbf{u}(t) + \mathbf{F}\mathbf{w}(t), \\ \mathbf{y}(t) &= \mathbf{C}\mathbf{X}(t) + \mathbf{v}(t). \end{aligned} \tag{38a,b}$$

The plant disturbance $\mathbf{w}(t)$ and sensor noise $\mathbf{v}(t)$ are both assumed to be stationary, zero mean, Gaussian with joint correlation function

$$E\left\{ \begin{bmatrix} \mathbf{w}(t) \\ \mathbf{v}(t) \end{bmatrix} [\mathbf{u}(t)\mathbf{v}(t)] \right\} = \begin{bmatrix} \Xi & 0 \\ 0 & \Theta \end{bmatrix} \delta(t-\tau), \tag{39}$$

where $E[.]$ denotes the expected value, δ denotes Dirac delta, and Ξ and Θ represent the intensities of the plant disturbance and the sensor noise. For the present case, Ξ and Θ are both defined to be positive definite.

The associated control input is obtained such that the system is stabilized and the control minimizes the cost function

$$J_{\mathrm{LQG}} = E\left\{ \int_0^\infty \left[\mathbf{x}^{\mathrm{T}}\mathbf{u}^{\mathrm{T}}\right] \begin{bmatrix} \mathbf{Z} & \mathbf{0} \\ \mathbf{0} & \mathbf{R} \end{bmatrix} \begin{bmatrix} \mathbf{x} \\ \mathbf{u} \end{bmatrix} \mathrm{d}t \right\}. \tag{40}$$

The optimal feedback gain matrix $\mathbf{K}$ and the Kalman filter gain matrix $\mathbf{L}$ are obtained from

$$\mathbf{K} = -\mathbf{R}^{-1}\mathbf{B}^{\mathrm{T}}\mathbf{P}, \quad \mathbf{L} = -\mathbf{\Pi}\mathbf{C}^{\mathrm{T}}\mathbf{\Theta}^{-1}, \tag{41a,b}$$

where $\mathbf{P}$ and $\mathbf{\Pi}$ are the positive definite solutions of the following Riccati equations:

$$\begin{aligned} &\mathbf{A}^{\mathrm{T}}\mathbf{P} - \mathbf{P}\mathbf{B}\mathbf{R}^{-1}\mathbf{B}^{\mathrm{T}}\mathbf{P} + \mathbf{Z} = 0 \\ &\mathbf{A}\mathbf{\Pi} + \mathbf{\Pi}\mathbf{C}^{\mathrm{T}}\mathbf{\Theta}^{-1}\mathbf{C}\mathbf{\Pi} + \mathbf{F}\mathbf{\Xi}\mathbf{F}^{-1} = 0. \end{aligned} \tag{42a,b}$$

Eq. (42b) reflects the fact that the design of Kalman filter is the dual problem to that of the full state feedback controller. It also results that the filter gain is determined based on statistical knowledge of the plant disturbance and noise measurements.

6.2. Sliding mode observer

The controller and the observer are designed based on the mathematical model that considers controlled modes only, whereas the output is formed from both controlled and residual (uncontrolled) modes. Since residual modes are not considered in the controller and observer design, their neglect may cause both control spillover and observation spillover. For evident reasons, it is desired to reduce the observation spillover as to remove the potential of generating any instability. To this end, we introduce a *sliding mode observer* which is known to have the robustness and the disturbance decoupling properties, this yielding a reduction of the effect of observation spillover from the residual modes, see Refs. [29,30], and also Ref. [31] where, in the latter paper the control methodology was applied to the case of a reusable space vehicle.

Considering the controlled mode system, Eq. (36a), the sliding mode observer has the form

$$\dot{\tilde{X}}_C(t) = \mathbf{A}_C\tilde{\mathbf{X}}_C + \mathbf{B}_C\mathbf{u}(t) + \mathbf{L}\left[\mathbf{y}(t) - \mathbf{C}_C\tilde{\mathbf{X}}_C(t)\right] + \mathbf{Y}\upsilon \tag{43}$$

where υ represents a discontinuous switching component defined as

$$\upsilon = \begin{cases} -\rho\dfrac{\mathbf{Pe}}{||\mathbf{Pe}||}, & \mathbf{e} \neq 0, \\ \mathbf{0}, & \mathbf{e} = 0. \end{cases} \tag{44}$$

The matrix $\mathbf{P}$ is a positive definite symmetric matrix that satisfies

$$\mathbf{P}\mathbf{A}_0 + \mathbf{A}_0^{\mathrm{T}}\mathbf{P} = -\mathbf{Q}, \tag{45}$$

where $\mathbf{A}_0 = \mathbf{A}_{\mathrm{C}} = \mathbf{L}\mathbf{C}_{\mathrm{C}}$; $\mathbf{Q}$ is a positive definite design matrix while ρ is a positive scalar function playing the role of a design parameter, and $\mathbf{e}(t)$ is the estimated error.

Table 1
Material properties and geometric specification of a wing with CAS lay-up and biconvex cross-section

E_L	$206.8 \times 10^9\ \mathrm{N/m^2}$
$E_L = E_T$	$5.17 \times 10^9\ \mathrm{N/m^2}$
G_{TT}	$3.10 \times 10^9\ \mathrm{N/m^2}$
$G_{LT} = G_{LT}$	$2.55 \times 10^9\ \mathrm{N/m^2}$
$\mu_{LT} = \mu_{LT} = \mu_{TT}$	0.25
ρ	$1.528 \times 10^3\ \mathrm{kg/m^3}$
Length (L)	6.058 m
Width ($2b$)	0.757 m
Depth ($2d$)	0.100 m
Aspect ratio	16
Wall thickness	0.003 m
Number of layers	6
Layer thickness	0.0005 m
Sweep angle (Λ)	0

Table 2
Eigenvalues of the system matrix A near the onset of flutter ($\theta = -75^\circ$)

$U_\infty = 138$ m/s (subcritical response)	$U_\infty = 138$ m/s (supercritical response)
-0.0315 ± 1.739j	-0.0315 ± 1.726j
-0.0340 ± 0.910j	-0.034 ± 0.903j
-0.0385 ± 0.560j	-0.039 ± 0.555j
-0.00362 ± 0.275j	0.00015 ± 0.273j
-0.101 ± 0.249j	-0.105 ± 0.249j
-0.291 ± 0.00635j	-0.291 ± 0.00646j
-0.300 ± 0.000506j	-0.300 ± 0.000513j
-0.0457 ± 0.000386j	-0.0457 ± 0.000392j
-0.0455	-0.0455
-0.0475	-0.0475
-0.0505	-0.505
-0.215	-0.214

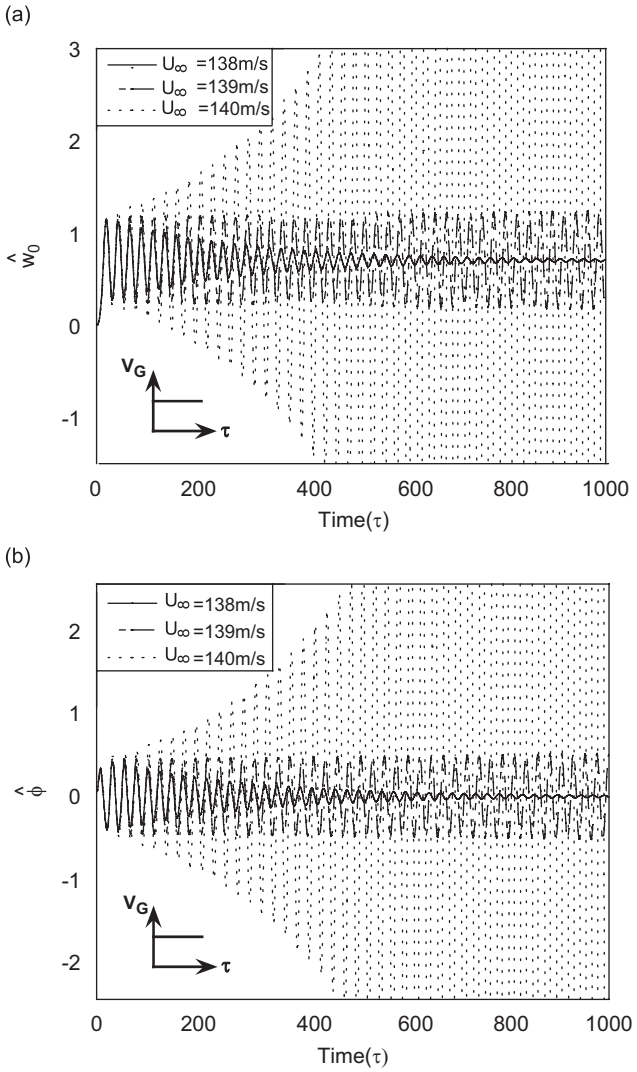

Fig. 2. Dynamic aeroelastic response of a wing ($\theta = -75^\circ$) subject to a sharp edged gust near the onset of flutter with parameters ($U_\infty = 138$, 139, 140 m/s): (a) plunging response (b) pitching response.

The objective is to induce a sliding motion in the error space

$$s_0 = \{e \in \mathbf{R}^n : \mathbf{C}_C\mathbf{e} = 0\}, \tag{46}$$

that produces an estimate $\tilde{X}_C$ of X_C, such that the error $\mathbf{e}(t) \to 0$ as $t \to \infty$, despite the presence of the uncertainties in modeling and plant disturbances. Considering that the output is composed of both the controlled modes and the residual modes, $y = C_C X_C + C_R X_R$, the dynamics of the estimated error becomes

$$\dot{\mathbf{e}} = \dot{\mathbf{X}}_C - \dot{\tilde{\mathbf{X}}}_C = \mathbf{A}_0\mathbf{e}(t) + \mathbf{Y}\upsilon + \mathbf{L}\mathbf{C}_R\mathbf{X}_R. \tag{47}$$

Note that the residual modes appear as a disturbance in the error dynamics. With the given form of additional discontinuous input, the sliding mode observer can estimate the states of the system as decoupling the effect of residual modes. For the stability of observation error dynamics including residual modes, using the Lyapunov stability theory (see e.g., Refs. [32]), it can be shown that the error dynamics is asymptotically stable.

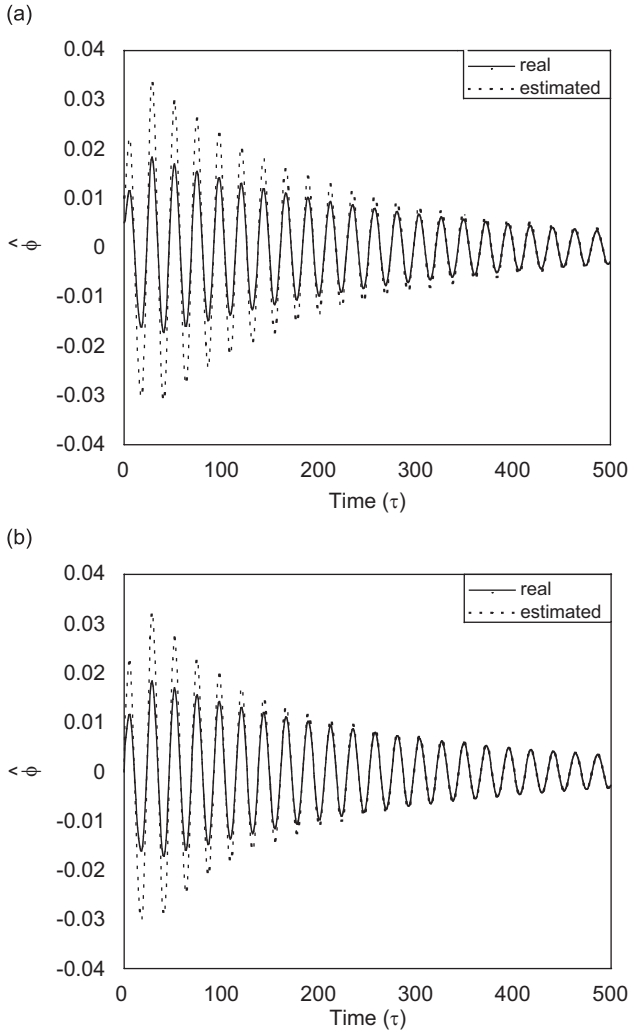

Fig. 3. Performance of state estimation using (b) sliding mode observer as compared to that based solely on (a) Kalman filter ($U_\infty = 138\,\mathrm{m/s}$).

7. Results and discussion

Unless otherwise stated, the geometrical and material characteristics of the wing that are used in the numerical simulations are supplied in Table 1. Note that in the actual simulations, the first five structural modes and two aerodynamic lag terms are used.

Wagner's function is approximated by Jones' quasi-polynomial formulas, and in the numerical simulations, all the response quantities, that is the dimensionless plunging, twist and transverse rotations are measured at the beam tip. In addition, unless otherwise specified, in the numerical simulations, the case of an unswept wing, $\Lambda = 0$ and the ply-angle $\theta = -75^\circ$, have been considered, where, (see Fig. 1), ply-angle θ is considered positive when measured from the positive circumferential coordinate s to the fiber direction, toward the positive span y-axis.

For this aeroelastic model, the flutter speed was obtained via the solution of both the complex eigenvalue problem and from the subcritical aeroelastic response analysis, and the related results are supplied in Table 2 and Fig. 2, respectively.

In Fig. 2, the open-loop dimensionless plunging, transverse shear and pitching time-histories for the aeroelastic system operating in three different flight speeds ($U_\infty = 138$, 139 and 140 m/s), and exposed to a sharp edged gust characterized by $V_G = 15$ m/s are presented. With the increase of the flight speed, an increase of the aeroelastic response amplitude is experienced. These results are simulated based on zero initial conditions.

Fig. 3 shows that for the case of the only first mode measurement available as a sensor output, the sliding mode observer finally produces stable pitching deflection estimates based on the measurement of first mode only and, consequently makes the system stable at the subcritical flight speed $U_\infty = 138$ m/s.

Fig. 4 represents the uncontrolled and controlled aeroelastic response of the wing tip under a sharp edged gust near the onset of flutter ($U_\infty = 138$, 140 m/s).

The results reveal the great efficiency of the adopted control methodology. Moreover, the results in Fig. 3 reveal that the SMO estimated predictions converge toward the real ones much faster than those based on Kalman Filter.

Fig. 5 displays the uncontrolled/controlled dimensionless aeroelastic response of a wing ($\theta = -75^\circ$) subjected to an explosive blast near the onset of flutter ($U_\infty = 138$, 140 m/s) based on first mode measurement only. The results reveal the excellent performance of the feedback control based on SMO.

The counterpart of Fig. 5 for the case of the system exposed to a symmetric sonic-boom ($r = 2$), is depicted in Fig. 6, and similar conclusions to those emerging from Fig. 5 can be reached. Herein, it is assumed that only

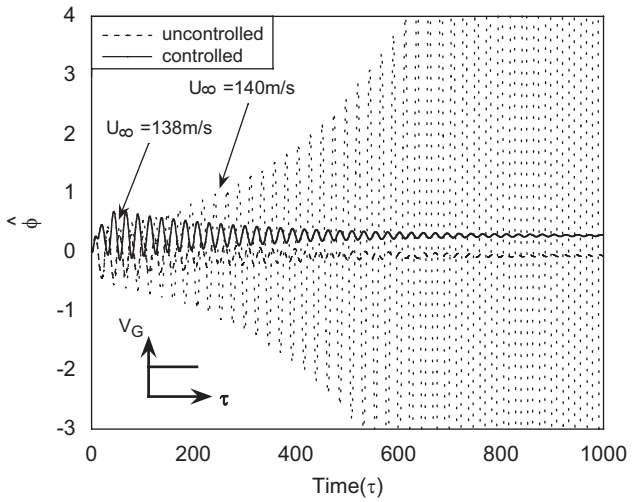

Fig. 4. Uncontrolled and controlled pitching aeroelastic response of a wing ($\theta = -75^\circ$) subjected to a sharp-edged gust near the onset of flutter ($U_\infty = 138$ m/s).

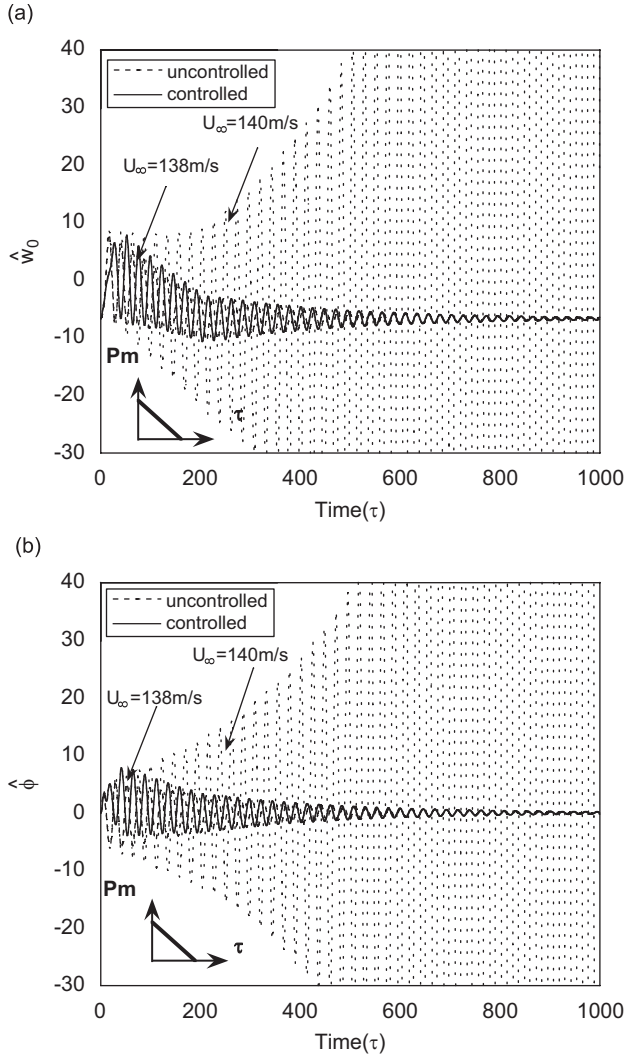

Fig. 5. Uncontrolled and controlled aeroelastic response of a wing ($\theta = -75^\circ$) subjected to an explosion blast the onset of flutter ($U_\infty = 140\,\mathrm{m/s}$, $\hat{P}_m = 1$, $\tau = 200$): (a) plunging response and (b) pitching response.

the first mode measurement is available. In addition to the high efficiency of the control, the results reveal that the closed-loop oscillation maximum response amplitude occurs in the free motion regime, that is for $\tau > 400$, when the explosive pulse has left the wing.

In Fig. 7, for a swept wing in a gas flow at a speed close to the flutter speed and subjected to a sharp-edge gust, it is shown that the positive wing swept angle can exert a beneficial influence on the aeroelastic response. In contrast to this, trend, for negative sweep angles, larger plunging amplitudes occur. In spite of this, the oscillations are much milder in the latter case than in the former one.

Finally, Fig. 8 shows the open-loop plunging time-history for the wing tip exposed to a sharp edged gust, for three selected ply-angles, when the flight speed is close to the flutter speed.

The results reveal that although for $\theta = 45^\circ$ the oscillation amplitude is larger than for $\theta = 60^\circ$ and 75°, in the former case the oscillations are completely damped in a short time, much shorter than for the other two ply-angles. These results reveal the efficiency of the aeroelastic tailoring toward the aeroelastic response.

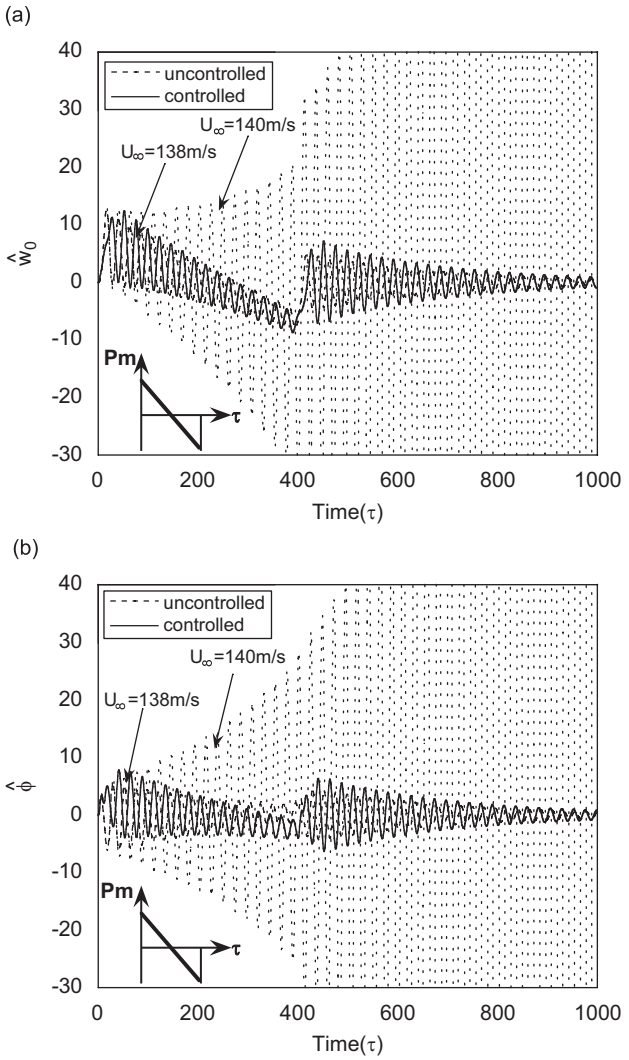

Fig. 6. Uncontrolled and controlled aeroelastic response of a wing ($\theta = -75^\circ$) subject to sonic boom near the onset of flutter ($U_\infty = 140\,\text{m/s}$, $\hat{P}_m = 1$, $\tau = 200$): (a) plunging response and (b) pitching response.

8. Conclusions

In this paper, a comprehensive aeroelastic model of anisotropic composite aircraft wings in the form of a thin/thick-walled beam considered in conjunction with a robust control methodology that yields an improvement of robustness to modeling uncertainties, external disturbances, and restricted sensor measurements was presented. The high efficiency of the implemented LQG control strategy using a sliding mode observer toward reducing the oscillation amplitudes generated by the impact of a blast pulse or by a gust, in the subcritical flight speed range, of expanding the flight envelope without weight penalties, and preventing the occurrence of the flutter instability penalties was demonstrated.

Although the developed structural model is proper to a high-aspect ratio wing, due to the incorporation of the warping inhibition, it can be applied to moderate to small aspect ratio wings, as well. For some results regarding the implications of the warping inhibition on static/dynamic response of cantilevered beams, the reader is referred to Ref. [33]. It should also be mentioned here that the preliminary results obtained by these authors reveal that this control methodology can be of great efficiency also in the compressible flight speed regime.

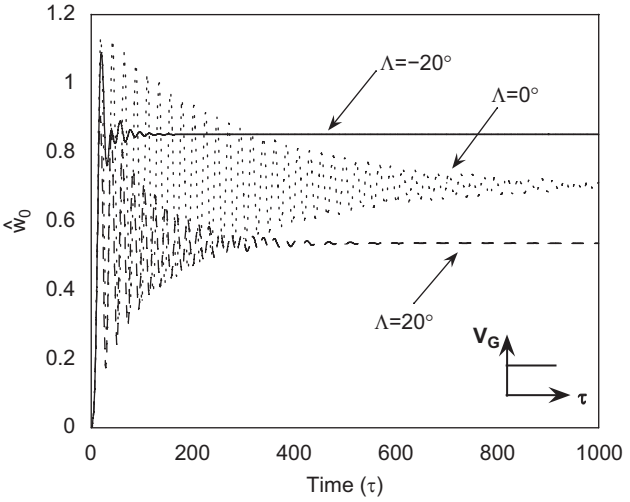

Fig. 7. Implication of the sweep angel on the aeroelastic in plunging subject to a sharp-edge gust near the onset of flutter ($U_\infty = 138\,\mathrm{m/s}$).

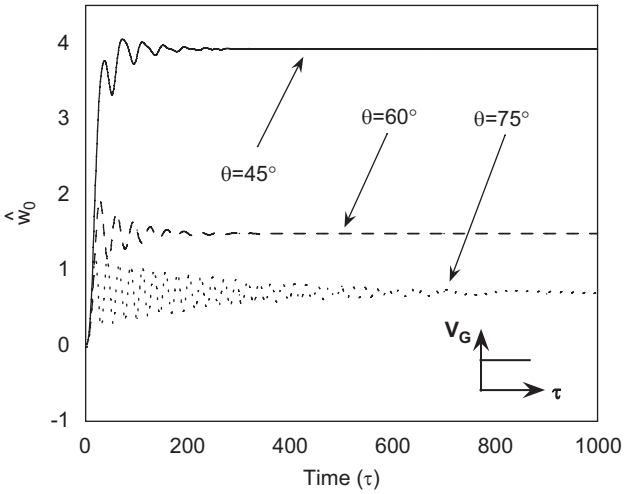

Fig. 8. Implications of the ply angle on the uncontrolled response of a wing subject to a sharp-edge gust near the inset of flutter ($U_\infty = 138\,\mathrm{m/s}$).

Acknowledgment

All the contributions and efforts of this work are dedicated to the memory of Professor Liviu Librescu (1930–2007) at VA Tech. S. Na acknowledges this work was supported by the Korea Science and Engineering Foundation grant funded by the Korea Government (No. R11-2007-00000-0).

References

[1] V. Mukhopadhyay, (Ed.), Benchmark active control technology, *Journal of Guidance, Control, and Dynamics* (2000–2001), Part I 23, 913–960; Part II 23, 1093–1139; Part III 24, 146–192.

[2] V. Mukhopadhyay, Historical perspective on analysis and control of aeroelastic responses, *Journal of Guidance, Control and Dynamics* 26 (5) (2003) 673–684.

[3] L. Librescu, P. Marzocca, Advances in the linear/nonlinear control of aeroelastic structural systems, *Acta Mechanica* 178 (3–4) (2005) 147–186.

[4] P. Marzocca, L. Librescu, G. Chiocchia, Aeroelastic response of 2-D lifting surfaces to gust and arbitrary explosive loading signatures, *International Journal of Impact Engineering* 25 (1) (2001) 41–65.
[5] P. Marzocca, L. Librescu, G. Chiocchia, Aeroelastic response of a 2-D airfoil in a compressible flow field and exposed to blast loading, *Aerospace Science and Technology* 6 (4) (2002) 259–272.
[6] L. Librescu, S. Na, P. Marzocca, C. Chung, M. Kwak, Active aeroelastic control of 2-D wing-flap systems operating in an incompressible flowfield and impacted by a blast pulse, *Journal of Sound and Vibration* 283 (3–5) (2005) 685–706.
[7] S.S. Na, L. Librescu, M.H. Kim, I.J. Jeong, P. Marzocca, Aeroelastic response of flapping wing systems using robust estimation control methodology, *Journal of Guidance, Control and Dynamics* 29 (1) (2006) 199–203.
[8] S.S. Na, L. Librescu, N.-H. Kim, I.-J. Jeong, P. Marcocca, Robust aeroelastic control of flapping wing systems using a sliding mode observer, *Journal of Aerospace Science and Technology* 10 (2006) 120–126.
[9] Z. Qin, L. Librescu, Aeroelastic instability of aircraft wings modeled as anisotropic composite thin-walled beams in incompressible flow, *Journal of Fluids and Structures* 19 (1) (2003) 43–61.
[10] L. Librescu, L. Meirovitch, O. Song, Refined structural modeling for enhancing vibrational and aeroelastic characteristics of composite aircraft wings, *La Recherche Aerospatial* 1 (1996) 23–35.
[11] Z. Qin, L. Librescu, Static and dynamic validations of a refined thin-walled composite beam model, *AIAA Journal* 39 (12) (2001).
[12] L. Librescu, O. Song, *Composite Thin-Walled Beams: Theory and Application*, Springer, 2005.
[13] G. Karpouzian, L. Librescu, Comprehensive model of anisotropic composite aircraft wings suitable for aeroelastic analyses, *Journal of Aircraft* 31 (3) (1994) 703–712.
[14] G. Karpouzian, L. Librescu, Non-classical effects on divergence and flutter of anisotropic swept aircraft wings, *AIAA Journal* 34 (4) (1996) 786–794.
[15] F.H. Gern, L. Librescu, Aeroelastic tailoring of composite aircraft wings exhibiting non-classical effects and carrying external stores, *Journal of Aircraft* 37 (6) (2000) 1097–1104.
[16] L.W. Rehfield, A.R. Atilgan, Toward understanding the tailoring mechanisms for thin-walled composite tubular beams, in: S.W. Tsai, J.M. Whiteny, T.W. Choi, R.M. Jones (Eds.). *Processing of the First USSR-USA Symposium on Mechanics of Composite Materials*, Riga, Catrai, USSR, May 23–26, ASME, 1989, pp. 187–196.
[17] Z. Qin, L. Librescu, Dynamic aeroelastic response of aircraft wings modeled as anisotropic thin-walled beams, *Journal of Aircraft* 40 (3) (2003) 532–543.
[18] T. Von Kármán, W.R. Sears, Airfoil theory for non-uniform motion, *Journal of the Aeronautical Science* 5 (10) (1938) 379–390.
[19] R.L. Bisplinghoff, H. Ashley, R.L. Halfman, *Aeroelasticity*, Dover, New York, 1996, pp. 217, 288–293, 397–399.
[20] J. Katz, A. Plotkin, *Low-Speed Aerodynamics: From Wing Theory to Panels Methods*, McGraw-Hill, New York, 1991, pp. 451–457.
[21] W.P. Rodden, B. Stahl, A strip method for prediction of damping in subsonic wind tunnel and flight flutter tests, *Journal of Aircraft* 6 (1) (1969) 9–17.
[22] E.C. Yates Jr., Calculation of Flutter Characteristics for Finite-Span Swept or Unswept Wings at Subsonic and Supersonic Speeds by a Modified Strip Analysis, RM L57L10, NACA, 1958.
[23] H.H. Flax, Aeroelasticity and flutter in high speed problems of aircraft and experimental methods, in: H.F. Donavan, H.R. Lawrence (Eds.), *High Speed Aerodynamics and Jet Propulsion*, Vol. VIII, Princeton University Press, 1961, pp. 161–417.
[24] L. Librescu, A. Nosier, Dynamic response of anisotropic composite panels to time-dependent external excitations, Paper ICAS-9001.4R, *17th Congress of the International Council of the Aeronautical Sciences*, Stockholm, Sweden, September 1990, pp. 2134–2144.
[25] L. Librescu, S.S. Na, Dynamic response of cantilevered thin-walled beams to blast and sonic-boom loadings, *Shock and Vibration* 5 (1) (1998) 23–33.
[26] L. Librescu, L. Meirovitch, S.S. Na, Control of cantilevers vibration via structural tailoring and adaptive materials, *AIAA Journal* 35 (8) (1997) 1309–1315.
[27] L. Meirovitch, *Principles and Techniques of Vibration*, Prentice-Hall, 1997, pp. 189–194, 206–210.
[28] M.J. Balas, Feedback control of flexible systems, *IEEE Transactions on Automatic Control* AC-23 (4) (1978) 673–679.
[29] C. Edwards, S. Spurgeon, *Sliding Mode Control: Theory and Applications*, Taylor & Francis, 1998.
[30] M.H. Kim, D.J. Inman, Reduction of observation spillover in vibration suppression using a sliding mode observer, *Journal of Vibration and Control* 7 (7) (2001) 1087–1105.
[31] C.E. Hall, Y.B. Shtessel, Sliding mode disturbance observer-based control for a reusable launch vehicle, *Journal of Guidance, Control, and Dynamics* 29 (6) (2006).
[32] S.H. Zak, *Systems and Control*, Oxford University Press, New York, Oxford, 2003.
[33] L. Librescu, Z. Qin, D.R. Ambur, Implications of warping restraint on statics and dynamics of elastically tailored thin-walled composite beams, *International Journal of Mechanical Sciences* 45 (8) (2003) 1247–1267.